Conformation and Lipid Binding of a C-Terminal (198−243) Peptide of Human Apolipoprotein A-I[†]

Hongli L. Zhu and David Atkinson*

Department of Physiology and Biophysics, Boston University School of Medicine, 715 Albany Street, Boston, Massachusetts 02118

Received August 22, 2006; Revised Manuscript Received November 21, 2006

ABSTRACT: Human apolipoprotein A-I (apoA-I) is the principle apolipoprotein of high-density lipoproteins that are critically involved in reverse cholesterol transport. The intrinsically flexibility of apoA-I has hindered studies of the structural and functional details of the protein. Our strategy is to study peptide models representing different regions of apoA-I. Our previous report on [1−44]apoA-I demonstrated that this N-terminal region is unstructured and folds into ∼60% α-helix with a moderate lipid binding affinity. We now present details of the conformation and lipid interaction of a C-terminal 46-residue peptide, [198−243]apoA-I, encompassing putative helix repeats 10 and 9 and the second half of repeat 8 from the C-terminus of apoA-I. Far-ultraviolet circular dichroism spectra show that [198−243]apoA-I is also unfolded in aqueous solution. However, self-association induces ∼50% α-helix in the peptide. The self-associated peptide exists mainly as a tetramer, as determined by native electrophoresis, cross-linking with glutaraldehyde, and unfolding data from circular dichroism (CD) and differential scanning calorimetry (DSC). In the presence of a number of lipid-mimicking detergents, above their CMC, ∼60% α-helix was induced in the peptide. In contrast, SDS, an anionic lipid-mimicking detergent, induced helical folding in the peptide at a concentration of ∼0.003% (∼100 μM), ∼70-fold below its typical CMC (0.17−0.23% or 6−8 mM). Both monomeric and tetrameric peptide can solubilize dimyristoylphosphatidylcholine (DMPC) liposomes and fold into ∼60% α-helix. Fractionation by density gradient ultracentrifugation and visualization by negative staining electromicroscopy demonstrated that the peptide binds to DMPC with a high affinity to form at least two sizes of relatively homogeneous discoidal HDL-like particles depending on the initial lipid:peptide ratio. The characteristics (lipid:peptide weight ratio, diameter, and density) of both complexes are similar to those of plasma A-I/DMPC complexes formed under similar conditions: small discoidal complexes (∼3:1 weight ratio, ∼110 Å, and ∼1.10 g/cm^3) formed at an initial 1:1 weight ratio and larger discoidal complexes (∼4.6:1 weight ratio, ∼165 Å, and ∼1.085 g/cm^3) formed at initial 4:1 weight ratio. The cross-linking data for the peptide on the complexes of two sizes is consistent with the calculated peptide numbers per particle. Compared to the ∼100 Å disk-like complex formed by the N-terminal peptide in which helical structure was insufficient to cover the disk edge by a single belt, the compositions of these two types of complexes formed by the C-terminal peptide are more consistent with a "double belt" model, similar to that proposed for full-length apoA-I. Thus, our data provide direct evidence that this C-terminal region of apoA-I is responsible for the self-association of apoA-I, and this C-terminal peptide model can mimic the interaction with the phospholipid of plasma apoA-I to form two sizes of homogeneous discoidal complexes and thus may be responsible for apoA-I function in the formation and maintenance of HDL subspecies in plasma.

The plasma concentration of high-density lipoprotein (HDL) is an inverse marker of potential cardiovascular disease. The well-documented anti-atherogenic function of HDL is related to its critical role in reverse cholesterol transport, such as mediation of cholesterol efflux from macrophage cells and inhibition of foam cell formation. Apolipoprotein A-I (apoA-I),[1] an exchangeable apolipoprotein with 243 amino acids, is the major protein component of HDL. The intrinsic flexibility of apoA-I allows its structure to adopt different conformations in different lipid environments. At least three distinct conformations of apoA-I, a lipid-free monomolecular or self-associated form, a less lipidated form of apoA-I as a component of nascent discoidal HDL, and a lipid-rich form of apoA-I as a component of mature spherical HDL, have been identified and are involved in the reverse cholesterol transport pathway.

Although plasma apoA-I probably exists in vivo predominantly in lipid-bound forms, understanding the structural and conformational changes between the lipid-free and different lipid-bound states is essential to understanding apoA-I

[†] This work was supported by Grant POHL26335 from the National Institutes of Health.

* To whom correspondence should be addressed: Department of Physiology and Biophysics, W308, Boston University School of Medicine, 715 Albany St., Boston, MA 02118-2526. Phone: (617) 638-4015. Fax: (617) 638-4041. E-mail: Atkinson@bu.edu.

[1] Abbreviations: apoA-I, apolipoprotein A-I; BOG, *n*-octyl β-D-glucopyranoside; far-UV CD, far-ultraviolet circular dichroism; CMC, critical micelle concentration; DMPC, dimyristoylphosphatidylcholine; EM, electron microscopy; PK, peak fraction; SDS, sodium dodecyl sulfate.

10.1021/bi061721z CCC: $37.00
Published on Web 01/18/2007

metabolism. Many different biophysical approaches have been utilized in investigating the structural conformation of apoA-I in lipid-free and different lipid-bound states (*1*, *2*).

A large number of apoA-I natural and constructed mutants have been reported and studied by us and others, as reviewed by Sorci-Thomas et al. (*3*). Many of the mutants have resulted in functional implications. ApoA-I mutants associated with hereditary amyloidosis are mainly localized around the N-terminus of apoA-I within residues 26−90, while mutants associated with low-plasma HDL are predominantly localized in the central domain within residues 143−166. Three domains have been proposed for mature human apoA-I: the N-terminal domain of residues 1−99, the central domain of residues 99−142 (or 99−186), and the C-terminal domain of residues 143−243 (or 186−243). The region of the "central domain" is not well-defined, partially due to the independent function of repeats 6 and 7 (residues 143−186) (*4*). It is generally accepted that the N-terminus is important for the stabilization of the lipid-free apoA-I conformation (*5*), the central domain (probably helix 5) is important for apoA-I to accommodate different amounts of phospholipids and thus to form different sizes of nascent discoidal HDL (*6*), the region of helix repeats 6 and 7 is required for LACT activation (*3*), and the extreme C-terminal domain (specifically helices 9 and 10) possesses the highest lipid binding affinity and thus may initiate the lipid binding of apoA-I (*7*−*10*).

The apoA-I conformation is mainly composed of amphipathic α-helices that are thought to bind lipid (*11*−*14*) and are formed by a 22-amino acid tandem repeat that can be further subclassified into two 11-residue repeats, A and B (*15*), in the exon 4-encoded region of the protein. The sequence of apoA-I contains various combinations of these A/B repeats (*15*). The structure of apoA-I (and other apolipoproteins) seems to be that of discrete folded repeats that function in a concerted fashion. A continuous helix repeat assignment describes 10 tandemly repeated helices punctuated mainly by prolines. However, although this continuous helical model is the most widely used one, assignment of the precise secondary structural distribution throughout the apoA-I sequence is far from being in agreement with different approaches (*11*, *15*−*22*).

Thus, studies of peptides (*15*, *23*−*25*) that model different regions of apoA-I can provide important information about the roles of specific residues and segments, and their interactions in the structure and stability of the parent apolipoprotein. Analysis of the consensus sequences of the A and B repeat derived from the sequences of multiple exchangeable apolipoproteins (*15*), together with studies of 44-residue consensus sequence peptides, showed ∼90 and ∼50% α-helical contents for peptides with ABAB (*26*) and ABBA (*27*) sequence ordering, respectively. Thus, repeat order and interhelical interaction between the 22-mer repeats play a role in stabilizing the folding of the 22-residue segments. A 44-residue helix hairpin unit may represent a fundamental cooperative unit in apoA-I, as suggested for apoC-I (*28*). This is also supported by our previous studies on terminal truncation mutants of apoA-I (*29*).

We are systematically characterizing the solution conformation and lipid interactions of a series of ∼44-residue peptides that represent the different arrangements of the A and B repeat motifs found in apoA-I. These include overlapping 44-residue peptides from the central domain [[99−142]-apoA-I, [121−164]apoA-I (*25*), and [143−186]apoA-I]. In addition, we have previously reported the unique properties of the N-terminal domain ([1−44]apoA-I) (*21*). Here we report the conformational characterization and studies of the phospholipid interactions of a peptide that represents the extreme C-terminal domain of apoA-I ([198−243]apoA-I). The sequence of this peptide encompasses the second half of putative helix 8, helix 9, and helix 10 and represents a unique BABB repeat motif. Interestingly, the recently determined crystal structure of apoA-I shows the first half of helix 8 to be unstructured, and the second half of helix 8 (starting from residue 197), helix 9, and helix 10 forms a helix hairpin structure that is an independent domain (*22*).

MATERIALS AND METHODS

Peptide Synthesis. [198−243]ApoA-I, acylated at the N-terminus and amidated at the C-terminus, was synthesized by Quality Controlled Biochemicals, Inc. (Hopkinton, MA), at purities of >95%. The purity of the peptide was further verified by mass spectroscopy. The experimentally determined molecular weight was 5244, consistent with the calculated molecular weight from the amino acid sequence of 5240.

Chemicals. All regular chemical reagents were purchased from Sigma. BOG [*n*-octyl β-D-glucopyranoside ($C_{14}H_{28}O_6$), MW = 292.37, 99%, nonionic detergent] was purchased from Dojindo Molecular Technologies, Inc. (Gaithersburg, MD). SDS [sodium dodecyl sulfate ($C_{12}H_{25}NaSO_4$), MW = 288.4, ultrapure 10% (w/v) in solution, anion−ionic detergent] was from Invitrogen. DMPC [dimyristoylphosphatidylcholine (C14:0), FW677.9] was from Sigma. DPC [dodecylphosphocholine (C12:0), MW = 351.47, alkyl phosphocholine, zwitterionic detergent] and DHPC [diheptanoylphosphatidylcholine (C6:0, $C_{20}H_{40}NO_8P$), MW = 453.51, zwitterionic detergent] were both from Avanti Polar Lipids, Inc. TFE [2,2,2-trifluoroethanol ($C_2H_3F_3O$), 99.9%, α-helix inducer] was purchased from Aldrich Chemical Co. (Milwaukee, WI, now Sigma-Aldrich). Glutaraldehyde (grade I 70%) was from Sigma-Aldrich (St. Louis, MO). DPPC [dipalmitoyl-1-^{14}C, MW = 734, 0.05 mCi/mL in a 1:1 toluene/ethanol mixture, 110 mCi/mM] was purchased from New England Nuclear (now Perkin-Elmer Life and Analytical Sciences, Inc., Boston, MA).

Circular Dichroism (CD) Spectroscopy. Far-UV CD spectra were recorded using an AVIV 62 DS spectropolarimeter, as described in detail previously (*21*). Briefly, the wavelength CD spectra were recorded from 250 to 190 or 185 nm and averaged over at least three consecutive scans. Melting curves were monitored at 222 nm (the negative CD band of an α-helix), with a 1.00 °C step size. Data were normalized to peptide concentration and expressed as molar ellipticity. The protein α-helical content was determined with 3% accuracy from the molar residue ellipticity at 222 nm (*30*).

Cross-Linking Peptide(s) and Plasma ApoA-I with Glutaraldehyde. Glutaraldehyde is a wide-range peptide cross-linker that forms covalent bonds with any two free NH_2 groups within a distance of ∼12 Å in solution (*31*). Like that of other cross-linkers, the cross-linking efficiency is dependent on the concentrations of both glutaraldehyde and

peptide. To determine the optimal cross-linking condition for each sample, glutaraldehyde was diluted at 0.0001, 0.001, 0.01, and 0.1%. The peptide was used at various concentrations from 0.5 to 2 mg/mL. The reaction was carried out at room temperature for 2 h. Excess glycine was added to stop the reaction for 3 min at room temperature. Tricine gels (from 10 to 20%) were used to separate the proteins.

Differential Scanning Calorimetry (DSC) Data Collection and Analysis. Excess heat capacity $C_p(T)$ of [198−243]apoA-I was measured using a VP-DSC microcalorimeter (MicroCal). The required sample volume was ∼600 μL. The concentrations of the peptide were from 0.5 to 2 mg/mL in 10 mM phosphate buffer at pH 7.4. Samples and/or buffer were heated and cooled at a scan rate of 30 K/h. Buffer baselines were recorded multiple times until the system reached a stable state. $C_p(T)$ data were recorded; buffer baselines were subtracted, and the data were normalized to monomer peptide concentration. Three fitting models provided by ORIGIN 7.0 were used to analyze the unfolding process of the peptide. ΔH_{cal} (calorimetry enthalpy) was determined directly from the DSC data using the monomer concentration. ΔH_v (vant Hoff enthalpy) was calculated from the equations for the models. The $\Delta H_v/\Delta H_{cal}$ ratio for each possible process was predicted: (1) $\Delta H_v/\Delta H_{cal} = 1$ for a two-state process (M ↔ U), (2) $\Delta H_v/\Delta H_{cal} = x \geq 2$ for the non-two-state process without dissociation (Ox ↔ I ↔ Ux), and (3) $\Delta H_v/\Delta H_{cal} \sim 2x/(x+1)$ for a non-two-state process with dissociation (Ox ↔ multiple states ↔ *x*U) (where M is the monomer in its native conformation, U is the unfolded state of the peptide, O is the oligomer of the peptide, I is an intermediate state between the folding state and unfolding state, and *x* is the number of peptides in the oligomer). Both the $\Delta H_v/\Delta H_{cal}$ ratio and the shape of the fitting curve were used to monitor the quality of a specific fitting.

Preparation of Reconstituted Discoidal HDL-like Particles. Freshly dissolved peptide in 10 mM phosphate buffer at pH 7.4 was used in all the experiments. Peptide−DMPC complexes were prepared by spontaneous association of the peptide with a turbid suspension of DMPC liposomes at 24 °C in phosphate buffer in a water bath for 24 h. To quantitate the lipid, a small amount of [^{14}C]DPPC (∼1:13000 DPPC:DMPC molar ratio) was mixed with DMPC in $CHCl_3$, dried under nitrogen, and further dried within a desiccator overnight before the preparation of peptide−DMPC complexes. A wide range of initial DMPC:[198−243]apoA-I ratios from 1:1 to 10:1 (w/w) were studied. After the solution became clear, it was used for CD experiments, density gradient fractionation, and/or EM visualization.

Density Gradient Ultracentrifugation. The density of the samples and the blank was adjusted to ∼1.2 g/mL using solid KBr, and the samples were spun at 50K rpm and 15 °C for 48 h. After the samples has been spun, 25 aliquots of 200 μL each were pipetted from the surface of the solution. For each fraction, the density was determined by refractive index, the amount peptide was determined by a modified Lowry assay, and the amount of lipid was determined by [^{14}C]DPPC scintillation counting, as described in detail previously (*21*). For each initial lipid:peptide weight ratio sample, the actual ratio of each fraction containing complexes was calculated from the measured lipid and peptide concentrations.

Electron Microscopy. [198−243]ApoA-I−DMPC complexes, simple mixtures, and peak fractions after density gradient separation were visualized by electron microscopy using the negative staining technique (*32*). Samples were observed on a CM12 electron microscope (Philips Electron Optics, Eindhoven, The Netherlands). Representative fields were photographed with an exposure time of 1.00 s, at 45000× magnification.

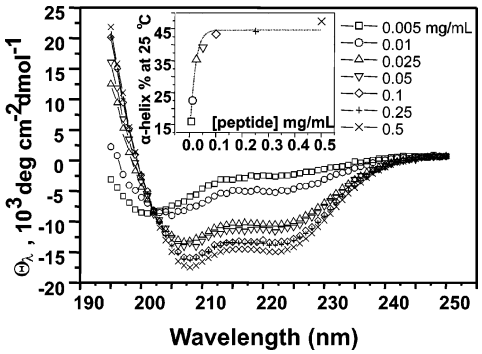

FIGURE 1: Far-UV CD spectra [$\theta(\lambda)$] of [198−243]apoA-I at (□) 0.005, (○) 0.01, (△) 0.025, (▽) 0.05, (◇) 0.1, (+) 0.25, and (×) 0.5 mg/mL. The samples were in 0.01 M phosphate at pH 7.4 and 25 °C. The inset shows the α-helical content of the peptide based on θ_{222}, as a function of peptide concentration.

Calculation of Discoidal Complex Compositions. The number of DMPC molecules per disc was estimated using the diameter of the discoidal complex from EM visualization, as described in detail previously (*21*). We assume a helix diameter of 10 Å and the surface area per DMPC of 65 Å^2 (*33*). The molar ratio of lipid to peptide for each fraction was determined from the lipid/peptide mass distribution in the density gradient.

RESULTS

Conformational Characterization of [198−243]ApoA-I in Solution. Figure 1 shows the far-UV CD spectra of [198−243]apoA-I over a 100-fold concentration range of 0.005−0.5 mg/mL. At the lowest concentration (∼5 μg/mL), a typical random coil spectrum with a minimum at 200 nm indicates that [198−243]apoA-I is unstructured in solution. The spectrum changes to that typical of an α-helix with minima at 208 and 222 nm as the peptide concentration increases, suggesting that self-association of [198−243]-apoA-I induces α-helical structure. The inset shows the α-helix content as a function of peptide concentration. At 5 μg/mL, both the ∼16% helical content and the overall unstructured nature of the spectrum suggest that [198−243]-apoA-I is probably monomeric. Self-association of [198−243]apoA-I starts at 0.01 mg/mL, and the α-helical content in the peptide reaches equilibrium at ∼0.1 mg/mL with the maximum helical content being ∼50%.

The self-association of [198−243]apoA-I was confirmed by native PhastGel electrophoresis. In contrast to the band at ∼5 kDa (Figure 2A) on SDS−PAGE, which corresponds to the molecular mass of the peptide (5244 Da), a single band at ∼20 kDa (Figure 2B) was observed on native gels, suggesting that the peptide was self-associated, probably into a tetramer. The self-association of the peptide was investigated further by cross-linking with glutaraldehyde (Figure 2C). At a peptide concentration of 1 mg/mL and the lowest cross-linker concentration (lane 5), a clear distribution of bands corresponding to the molecular mass of monomer, dimer, and trimer, together with two closely spaced bands

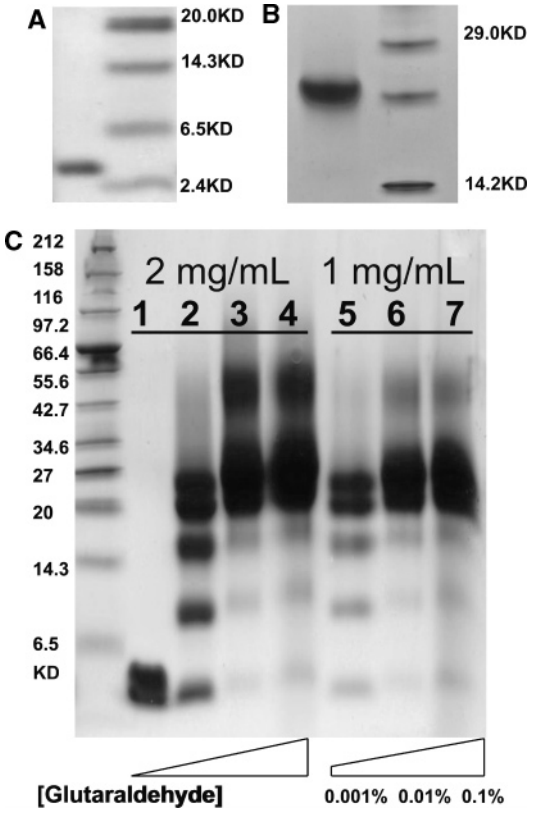

FIGURE 2: Electrophoresis studies on [198−243]apoA-I in solution: (A) 1 mg/mL [198−243]apoA-I in solution, separated via SDS−PAGE, (B) 1 mg/mL [198−243]apoA-I in solution, separated with a native 4−15% Phast Gel, and (C) glutaraldehyde cross-linked peptides in solution, separated on a 10−20% Tricine gradient gel. The concentrations of glutaraldehyde were (lane 1) 0%, (lanes 2 and 5) 0.001%, (lanes 3 and 6) 0.01%, and (lanes 4 and 7) 0.1%. Peptide concentrations were 2 mg/mL from lane 1 to 4 and 1 mg/mL from lane 5 to 7.

corresponding to tetramer and possibly pentamer, was observed. The two bands around ∼21 kDa in lane 5 were identified as the tetramer and pentamer of the peptide by MALDI-TOF mass spectrometry (data not shown). At the same peptide concentration, tetramer and maybe pentamer became predominant and lower species (monomer, dimer, and trimer) became less pronounced, as the cross-linker concentration increased (lanes 6 and 7). Similar characteristics were observed for the peptide at higher concentrations (lanes 3 and 4), except that larger oligomer species appeared at a molecular range of ∼50 kDa (lanes 3 and 4). These higher species probably result from the nonspecific cross-linking between the predominant peptide aggregates (i.e., tetramer and/or pentamer). However, the small oligomer species were still observed, even in the presence of excess cross-linker (lanes 4 and 7). This could result from either low cross-linker efficiency or the existence of an equilibrium between multiple self-associated states of the peptide in solution.

Figure 3A shows the thermal unfolding of [198−243]-apoA-I at five concentrations from 0.025 to 0.5 mg/mL. At each peptide concentration, both thermal unfolding measurements from 0 to 95 °C and immediate reverse scans from 95 to 0 °C are shown by the same symbol. At low concentrations, 0.025 and 0.05 mg/mL specifically, the reverse scans were slightly separated from the heating curves, with the heating curve below and the cooling curve above. However, three successive heating and cooling scans of the same sample at 0.025 mg/mL (0 °C ↔ 50 °C, 0 °C ↔ 60 °C, and 0 °C ↔ 80 °C) completely overlapped (data not shown). This suggests that the slight helix loss observed in the reverse scan at 0.025 mg/mL from 95 to 0 °C is probably due to the permanent denaturation of a small amount of [198−243]apoA-I at high temperatures. Peptide concentration determination confirmed the loss of the peptide from being heated at high temperature. Thus, the thermal unfolding of the peptide at all measured concentrations is reversible.

At all concentrations, the peptide undergoes apparent loss of α-helical structure at both high and low temperatures, with a maximum α-helix content at ∼20 °C. Since hydrophobic self-association is temperature-dependent and strongest at room temperature (*34*), the apparent loss of helical structure at low temperatures is probably the result of a decrease in the level of self-association of the peptide.

Figure 3B shows the thermal unfolding of [198−243]-apoA-I at five concentrations with a slower scan rate (0.00033 K/s or 300 s/K) starting at room temperature. The reverse scans overlapped with their corresponding heating curves and are not shown for clarity. Interestingly, at 25 °C and all peptide concentrations that were examined except the lowest (0.0125 mg/mL), the α-helical contents of the peptide at different concentrations were similar, in contrast to those shown in Figure 3A where the starting temperature was 0 °C. This indicates that the apparent unfolding process of the self-associated peptide at low temperatures (0−25 °C) is probably a kinetically controlled process that results from both the decrease in the level of self-association and the thermal unfolding of the peptide.

At 0.0125 mg/mL, where the α-helix content was ∼38%, the unfolding curve of [198−243]apoA-I was sigmoidal, suggesting a cooperative two-state process. However, the unfolding curve became less cooperative in appearance as the peptide concentration increased. At a concentration of 0.5 mg/mL, the nonsigmoidal shape of the peptide unfolding process suggests the existence of multiple steps between the folded state and the unfolded state. The apparent T_m (Figure 3C), derived from data in Figure 3B, shifts to a higher temperature by ∼40 °C as the peptide concentration increases from 0.0125 mg/mL (∼54 °C) to 0.5 mg/mL (∼85−92 °C). This suggests the formation of higher oligomer states at higher peptide concentrations, with the higher self-associated oligomers being more stable.

The self-association of the peptide was investigated further by differential scanning calorimetry (DSC) measurements of the thermal unfolding at three peptide concentrations, 1, 2, and 3 mg/mL. At 1 mg/mL, a sharp transition was observed at high temperatures with a T_m of ∼97 °C (Figure 3D). This T_m is significantly higher (∼5 °C) than that measured in CD experiments for the peptide at 0.5 mg/mL. At peptide concentrations of 2 and 3 mg/mL, the measured T_m did not change significantly, suggesting that self-association of the peptide reached equilibrium at a concentration of 1 mg/mL. A tetramer dissociation model yielded the best fitting to the sharp peak at high temperatures (as shown in Figure 3D). Alternative models, including a two-state model, a non-two-state model, and a non-two-state other oligomer dissociation (see Materials and Methods), were inadequate in describing the data. The broad peaks at low temperatures probably correspond to unfolding and/or dis-

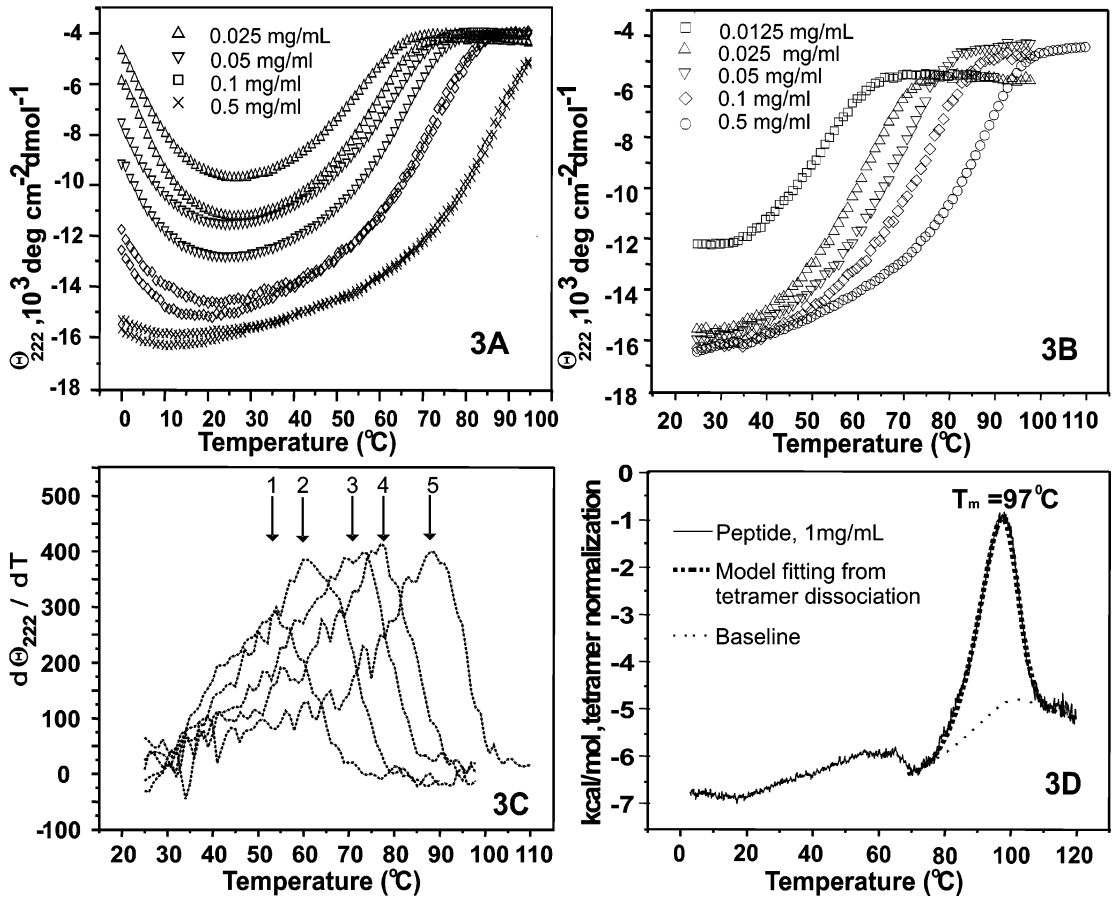

FIGURE 3: (A) Thermal unfolding spectra [$\theta_{222}(T)$] of [198−243]apoA-I as a function of peptide concentration. The temperature range was from 1 to 95 °C. The two lines show heating and cooling. The scanning rate was 0.0167 K/s (60 s/K). Four peptide concentrations are shown: (△) 0.025, (▽) 0.05, (□) 0.1, and (×) 0.5 mg/mL. (B) Thermal unfolding spectra [$\theta_{222}(T)$] of [198−243]apoA-I, starting from 25 °C to its unfolded state at a lower scan rate of 0.0033 K/s (300 s/K). Five peptide concentrations are shown: (□) 0.0125, (△) 0.025, (▽) 0.05, (◇) 0.1, and (○) 0.5 mg/mL. (C) Differentiation analysis of data in panel A. $d\theta_{222}(T)/dT$ as a function of temperature. The corresponding peptide concentration and apparent T_m (marked by the arrows) for the five curves from left to right are as follows: (1) 0.0125 mg/mL and ∼54 °C, (2) 0.025 mg/mL and ∼61 °C, (3) 0.05 mg/mL and ∼70−75 °C, (4) 0.1 mg/mL and ∼75−80 °C, and (5) 0.5 mg/mL and ∼80−92 °C, respectively. (D) Differential scanning calorimetry (DSC) of 1 mg/mL [198−243]apoA-I with a heating rate of 0.0083 K/s (30 K/h). The best fitting with a non-two-state tetramer dissociation model is shown: (—) normalized data from DSC measurement and (···) baseline generated by the fitting model and (- - -) fitting curve. The buffer line was subtracted. Only the larger peak at high temperatures was analyzed. The baseline was initiated according to the shape and further refined by the fitting model.

sociation the lower self-associated oligomers, such as dimer and trimer.

Thus, in solution, the peptide is in self-association equilibrium between monomer and multiple oligomeric states, including dimer, trimer, tetramer, and maybe pentamer. At a low peptide concentration (0.0125 mg/mL), the equilibrium is probably dominated by unfolded monomer and folded dimer, and the thermal unfolding process of the peptide at this concentration is close to a two-state cooperative process. As the concentration increases, trimer, tetramer, and maybe pentamer are formed by further self-association. Tetramer becomes predominant as suggested by the DSC data. Thus, after the self-association reaches equilibrium, the major species and the most stable species is tetramer.

Interaction with Detergent and Folding Reagents. A number of detergents, BOG (a small nonionic lipid-mimicking detergent), SDS (an anionic detergent), DPC (a single-chain phospholipid zwitterionic detergent), and DHPC (a double-short chain zwitterionic detergent) together with TFE (an α-helix inducer) induced the unstructured monomeric [198−243]apoA-I to fold into ∼60% α-helix. In the presence of all nonionic detergents, BOG, DPC, and DHPC, at and above their CMC, far-UV CD spectra (data not shown) exhibited pronounced minima at 208 and 222 nm, typical of α-helix. Figure 4A shows the example of the α-helical content of [198−243]apoA-I at 25 °C, as a function of BOG concentration. The level of α-helical structure in [198−243]-apoA-I increased rapidly as the concentration of BOG increased in a small range around its CMC [∼0.6% (*35*)] from 0.2 to 0.8% and reached its maximum of ∼60% at and above 0.8% BOG.

In contrast, in the presence of the ionic detergent SDS, the unstructured monomeric peptide started to form α-helix in 0.0004% SDS, ∼500-fold below the typical CMC [0.17−0.23% (*36*, *37*)] of the detergent. Figure 4B shows the α-helical content of [198−243]apoA-I at 25 °C over a wide SDS concentration range from 0.0002 to 0.25% (note that there is a break in the *x*-axis to show clearly the data at low SDS concentrations). At low SDS concentrations, from 0.0002 to 0.0024% with a midpoint of 0.001% (35 μM), the α-helical content of the peptide increased dramatically as the SDS concentration increased. This effective SDS concentration did not change over a 10-fold peptide concentration range (0.005−0.05 mg/mL, data not shown). Thus, SDS

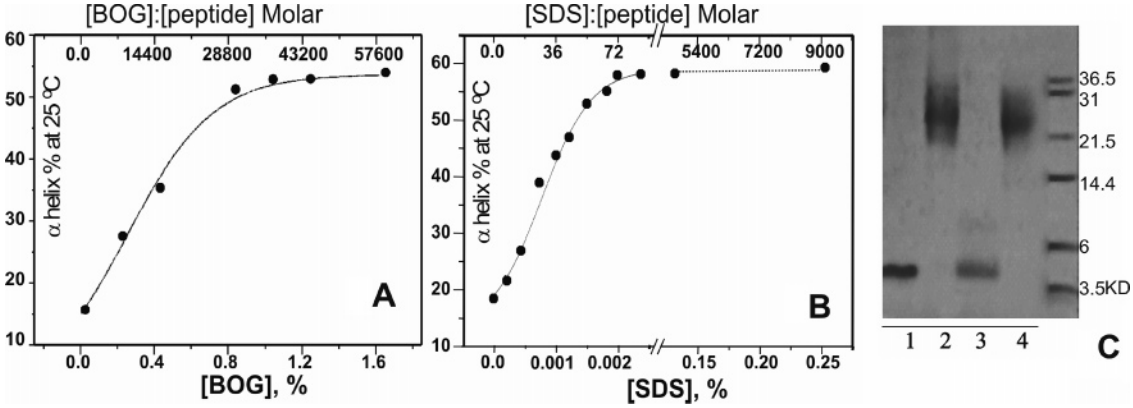

FIGURE 4: (A) α-Helical percentage of [198−243]apoA-I on the basis of θ_{222}, as a function of BOG concentration. The peptide concentration was 0.005 mg/mL. The concentrations of BOG from left to right were 0, 0.2, 0.4, 0.8, 1.0, 1.2, and 1.6%. The corresponding BOG:peptide molar ratios are displayed on the top axis. (B) α-Helical percentage of [198−243]apoA-I on the basis of θ_{222}, as a function of SDS concentration. The peptide concentration was 0.005 mg/mL. The concentrations of SDS from left to right were 0, 0.0002, 0.0004, 0.0008, 0.001, 0.0012, 0.0014, 0.0018, 0.002, 0.0024, 0.125, and 0.25%. The corresponding SDS:peptide molar ratios are shown on the top axis. (C) Cross-linking of [198−243]apoA-I in the presence of various amounts of SDS. The peptide concentration was 1 mg/mL. Lane 1 contained no SDS with no cross-linker as a control, lane 2 no SDS and 0.01% glutaraldehyde, lane 3 0.2% SDS (typical CMC) and 0.01% glutaraldehyde, and lane 4 0.02% SDS (∼10-fold below its typical CMC but high enough to induce the formation of α-helical structure in [198−243]apoA-I) and 0.01% glutaraldehyde.

induces α-helical structure in [198−243]apoA-I at a concentration ∼70-fold lower than its typical CMC, suggesting that the α-helix formation in the peptide is either due to the SDS micelle formation at much lower concentration than in the absence of the peptide or due to the specific binding of monomeric SDS to the peptide.

The SDS concentration, where the half-maximal amount of α-helix was induced in [198−243]apoA-I, was ∼0.001% (∼35 μM), which corresponds to a SDS:peptide molar ratio of 36:1 for a peptide concentration of 0.005 mg/mL (top *x*-axis in Figure 4B). In contrast, in the presence of BOG, a nonionic detergent with a molecular weight and micelle aggregation number [∼84 (*35*)] similar to those of SDS, the equivalent detergent:peptide value for the 0.005 mg/mL peptide was much larger (14400:1 molar ratio, top *x*-axis in Figure 4A). Since the effective SDS concentration range is independent of peptide concentration (data not shown), at a peptide concentration of 0.05 mg/mL, the SDS:peptide molar ratio will be ∼3.6:1. A typical aggregation number for SDS spherical micelles is ∼60 (*38*). Thus, for [198−243]apoA-I in the presence of the SDS concentration where α-helical structure was induced, there were insufficient micelles for each peptide molecule even if the SDS micelles could be formed at such a low concentration. Therefore, single molecules of SDS may bind specifically to the peptide and induce the formation of α-helical structure, which is in contrast to the current concept (*19*) that SDS micelles induce and stabilize α-helical structure in apolipoproteins.

Since both self-association and SDS induced the formation of α-helical structure in the peptide, a cross-linking study of the interaction of self-associated (1 mg/mL) [198−243]-apoA-I at different SDS concentrations was carried out (Figure 4C). In the presence of 0.2% SDS (typical CMC) and 0.01% cross-linker (lane 3), a single band corresponding to monomer was observed, demonstrating that the SDS micelles disrupted the self-association of [198−243]apoA-I. Whereas in the presence of 0.02% SDS (lane 4), a concentration ∼10-fold below the typical CMC of SDS but enough to induce additional ∼10% α-helical structure (data not shown) in self-associated [198−243]apoA-I, the peptide remained in its tetrameric form. Thus, at submicellar concentrations, SDS induced slightly more α-helical structure without disrupting the oligomerization of the peptide, maybe through specific binding.

Lipid Binding of [198−243]ApoA-I. [198−243]ApoA-I solubilized DMPC liposomes over a wide range of initial DMPC:[198−243]apoA-I ratios from 1:1 to 10:1 (w/w). Similar to the observations in the presence of detergents, unstructured monomeric [198−243]apoA-I (0.005 mg/mL) folded into α-helix in a DMPC concentration-dependent manner and reached an apparent maximum α-helix content at a >4:1 (w/w) DMPC:[198−243]apoA-I ratio. The apparent α-helical content for [198−243]apoA-I in DMPC was ∼60% (inset of Figure 5B). At 0.1 mg/mL or a higher peptide concentration when self-association induced ∼50% α-helix, the helical amount did not increase significantly.

DMPC−[198−243]apoA-I complexes at three initial DMPC:peptide ratios, 1:1, 4:1, and 8:1 (w/w), were separated by density gradient ultracentrifugation and the peak fractions visualized by EM. Figure 5A shows the lipid distribution, and Figure 5B shows the peptide distribution in the density gradient. In all cases, the lipid peak fraction corresponded to the peptide peak fraction except at an initial 1:1 (w/w) ratio, which showed a one-fraction shift of the lipid to the lower density range. All DMPC, together with most peptide, was enriched at a higher density range than that for free lipid, covering three to five fractions of 25 in total, demonstrating complex formation. No free [198−243]apoA-I was observed at and above an initial 4:1 (w/w) ratio. Weight ratios, derived from panels A and B of Figure 5 for those fractions containing a significant amount of complex, are shown in Figure 5C. For the initial 1:1 ratio, relatively uniform ∼3:1 weight ratio complexes were formed, and for the initial 4:1 ratio, relatively uniform ∼4.6:1 weight ratio complexes were formed. For the initial 8:1 ratio, rather heterogeneous particles were formed. At and above an initial 4:1 ratio, the peak ratio was similar to the initial ratio.

After density gradient ultracentrifugal separation, three to five fractions encompassing the peak for each sample were visualized individually by EM. For initial 1:1 and 4:1 ratios,

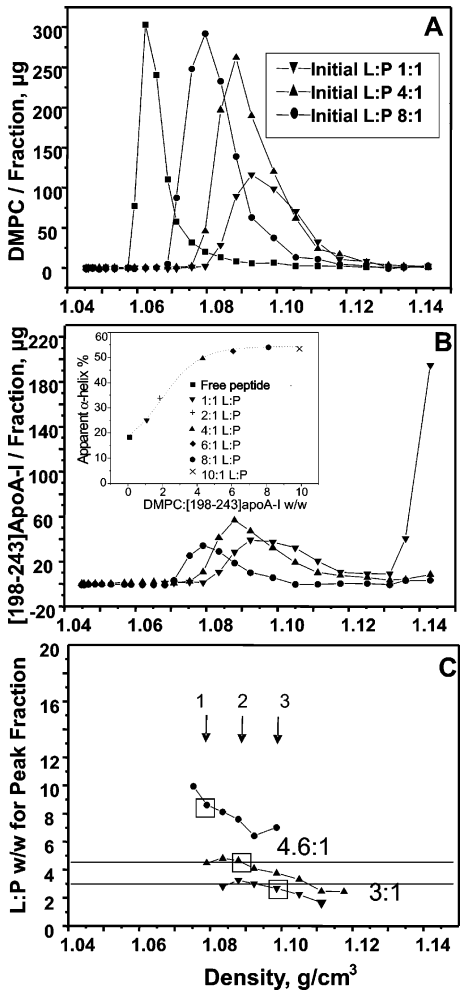

FIGURE 5: Density gradient ultracentrifugation of [198−243]apoA-I−DMPC mixtures at three initial lipid:peptide (L:P) ratios (w/w): 1:1, 4:1, and 8:1. (A) DMPC distribution in the density gradient: (▼) 1:1, (▲) 4:1, (●) 8:1, and (■) DMPC alone. (B) Corresponding peptide distribution in the density gradient. Symbols are the same as in panel A. The inset shows the apparent α-helical percentage of the [198−243]apoA-I−DMPC complex from simple mixtures of peptide and DMPC at different DMPC:[198−243]apoA-I ratios (w/w) with a peptide concentration of 0.005 mg/mL at pH 7.4 and 25 °C: (■) no lipid, (▼) 1:1, (+) 2:1, (▲) 4:1, (◆) 6:1, (●) 8:1, and (×) 10:1. (C) Corresponding DMPC:[198−243]apoA-I ratio (w/w) for each fraction that contains complexes as a function of density. Symbols are the same as in panel A. The arrows and boxes marked the peak fraction of each initial ratio: (1) 1:1, (2) 4:1, and (3) 8:1.

the morphology of the complexes in all the fractions was similar. Typical discoidal complexes were observed individually, en face, on edge, and stacked in rouleaux. A representative EM micrograph of the peak fraction at ∼1.1 g/cm^3 from an initial 1:1 ratio sample is shown at the right, and the corresponding size distribution is shown on the left in Figure 6A. Homogeneous complexes, with a mean diameter of ∼110 (108 ± 19) Å and a thickness of ∼50 Å, typical of a single-phospholipid bilayer, were observed. For the peak fraction at an initial 4:1 ratio at 1.085 g/cm^3 (Figure 6B), a larger homogeneous complex, with a mean diameter of ∼165 (162 ± 27) Å and the thickness of a single-phospholipid bilayer, was observed. For an initial DMPC:[198−243]apoA-I ratio of 8:1 (w/w) (data not shown), both larger disks and vesicles were observed in the peak fraction.

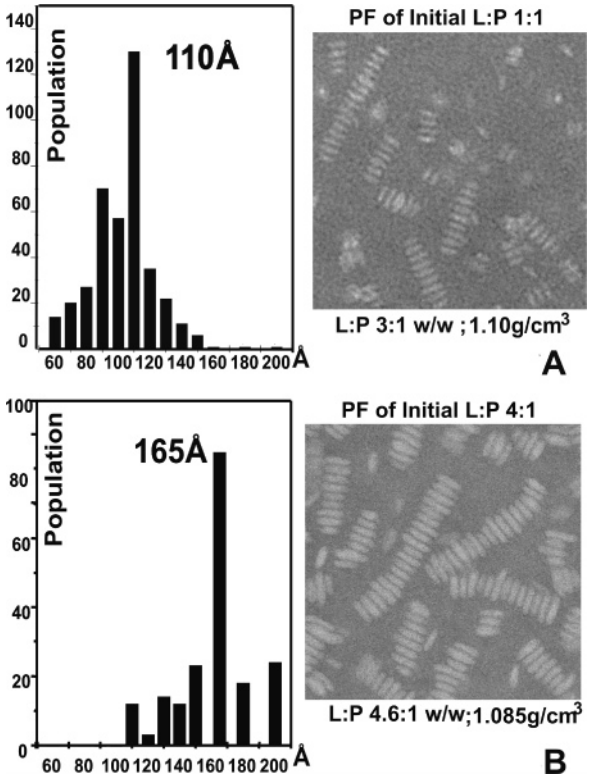

FIGURE 6: Negative staining EM images at 45000× magnification observation of the peak fractions for two initial DMPC−[198−243]apoA-I samples and their corresponding size distributions: (A) 1:1, mean ± SD = 108 ± 19 Å and (B) 4:1, mean ± SD = 162 ± 27 Å.

Vesicles were predominant in fractions at lower densities and more disklike particles in fractions at higher densities.

The compositions of the discoidal particles, calculated from the combination of weight ratio and size (see Materials and Methods for calculation), are ∼8 peptide and ∼200 DMPC molecules for small disks (∼110 Å) formed at an initial lipid:peptide ratio of 1:1 and ∼14 peptide and ∼500 DMPC molecules for large disks (∼165 Å) formed at an initial ratio of 4:1.

To determine the number of peptide molecules per disk directly, peptide molecules on the same complex were cross-linked by glutaraldehyde. As shown in Figure 7, the simple 1:1 (w/w) mixture of DMPC and [198−243]apoA-I (lane 2 in panel C) with a predominant size of ∼110 Å from EM observations (Figure 6A) resulted in a broad band around ∼40−55 kDa corresponding to ∼8−10 peptide molecules. The peak fraction of the 4:1 (w/w) DMPC−[198−243]apoA-I complex (lane 2 in panel D) with a predominant size of ∼165 Å from EM observations (Figure 6B) exhibited a broad band around ∼70−90 kDa, corresponding to ∼14−18 peptide molecules. Thus, for both types of disks formed by the C-terminal peptide, the peptide numbers per disk estimated from cross-linking were close to those calculated from the mean weight ratio and the size measured in EM observations.

A simple 4:1 (w/w) mixture of DMPC and plasma A-I (panel B in Figure 7), containing a mixture of both small (∼110 Å) and large (∼165 Å) disks observed at the peak fraction (*32*, *39*), was used for comparison. In the presence of a cross-linker, the molecular masses of the two pronounced bands (lane 3 in panel B), ∼55 kDa for two cross-linked

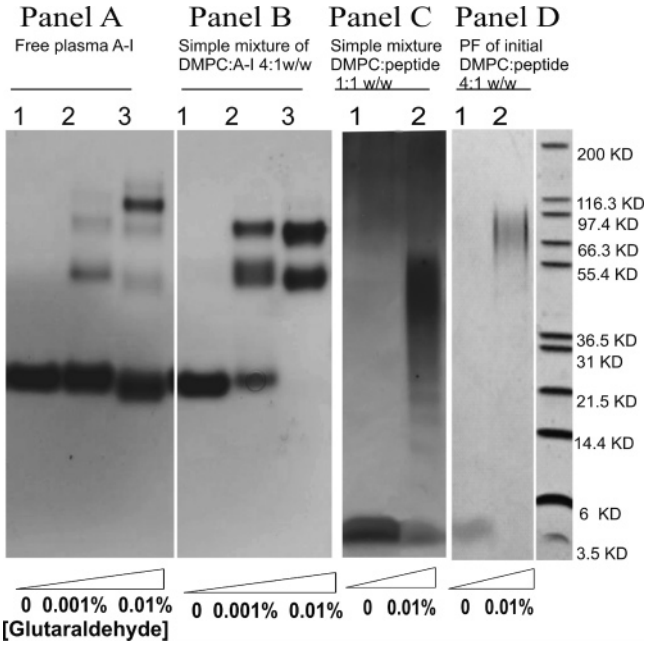

FIGURE 7: Glutaraldehyde-cross-linked peptide−protein complexes of the protein−DMPC complexes, separated with a 10−20% Tricine gradient gel. Panel A is for 0.8 mg/mL apoA-I in solution. The concentrations of glutaraldehyde were (lane 1) 0%, (lane 2) 0.001%, and (lane 3) 0.01%. Panel B is for 0.8 mg/mL plasma A-I in complex with DMPC from a 4:1 (w/w) lipid/protein simple mixture. The concentrations of cross-linker were the same as in panel A. Panel C is for 0.8 mg/mL [198−243]apoA-I complexed with DMPC from a 1:1 (w/w) lipid/peptide simple mixture: (lane 1) no cross-linker and (lane 2) 0.01% glutaraldehyde. Panel D is for 0.8 mg/mL [198−243]apoA-I in the peak fraction of the initial 4:1 (w/w) DMPC/peptide mixture: (lane 1) no glutaraldehyde and (lane 2) 0.01% glutaraldehyde. Panel C was silver stained to show the protein bands.

A-I molecules from small disks (∼110 Å) and ∼80 kDa for three cross-linked A-I molecules from the large disks (∼165 Å), are similar to those for the complexes formed by the C-terminal peptide. Thus, the C-terminal peptide [198−243]-apoA-I can interact with DMPC liposomes to generate two sizes of discoidal HDL-like complexes, both of which are similar to the disks formed by plasma A-I under similar conditions. Therefore, [198−243]apoA-I can mimic the lipid interaction of the intact A-I.

Stability of Complexes Formed by [198−243]ApoA-I and DMPC. To compare the stability of complexes formed by [198−243]apoA-I and apoA-I with DMPC, both thermal unfolding [$\theta_{222}(T)$, Figure 8A] and temperature-jump [$\theta_{222}(t)$, Figure 8B] experiments were performed for initial 4:1 (w/w) lipid/peptide or lipid/protein mixtures. The peptide representing the N-terminal apoA-I ([1−44]apoA-I), as characterized previously (*21*), was also investigated. The apparent T_m was ∼50 °C for the 4:1 (w/w) DMPC−[1−44]-apoA-I complex, ∼65 °C for the 4:1 (w/w) DMPC−[198−243]apoA-I complex, and ∼82 °C for the 4:1 (w/w) DMPC−apoA-I complex (Figure 8A), derived from the differential analysis of the thermal unfolding heating curves at the same scanning rate. Thus, the apparent stabilities of the reconstituted particles are as follows: 4:1 (w/w) DMPC−apoA-I > 4:1 (w/w) DMPC−[198−243]apoA-I > 4:1 (w/w) DMPC−[1−44]apoA-I.

Temperature-jump $\theta_{222}(t)$ data for the three types of mixtures at 4:1 (w/w) DMPC:peptide or DMPC:protein ratios, from 25 to 75 °C, showed a significant difference in the unfolding rates (Figure 8B). At 75 °C, it took ∼1−2 min for the [1−44]apoA-I−DMPC complex, ∼2 h for the [198−243]apoA-I−DMPC complex, and ∼16 h for the plasma A-I−DMPC complex to fully unfold. Thus, the differences in the unfolding rates for the same temperature jump for the three types of complexes were consistent with the apparent T_m derived from thermal unfolding. Under similar conditions, the C-terminal peptide of apoA-I ([198−243]apoA-I) formed a more stable complex with DMPC than the N-terminal peptide ([1−44]apoA-I), which is consistent with the high lipid affinity of [198−243]apoA-I. In addition, both the peptides formed significantly less stable complexes than intact apoA-I. This suggests that inter-repeat interactions of apoA-I are important in the stabilization of the helical structure of intact apoA-I on discoidal complexes and thus plasma HDL.

DISCUSSION

Solution Structure. [198−243]ApoA-I is unstructured in solution at a concentration of ∼1 μM (0.005 mg/mL, Figure 1). Previous studies on other peptides in our laboratory, [1−44]apoA-I (*21*), [99−142]apoA-I, and [121−164]apoA-I, have also shown that they are all unstructured (*25*). [143−186]ApoA-I is also unstructured over a concentration range from 0.02 to 0.2 mg/mL, although there is a tendency for the peptide to form a dimer at and above ∼1 mg/mL (data not shown). The five peptides cover regions of the N-terminal, C-terminal, and central segment, encompassing 178 residues of the total of 243 amino acids of intact apoA-I. However, intact apoA-I in solution has ∼60% α-helical structure, even at a concentration of 2 μM (0.005 mg/mL) when the protein is fully monomeric. This suggests that the interaction of the helix repeats contributes to the folding of apoA-I into α-helical structure and stabilizes lipid-free apoA-I. The C-terminal region in the monomeric intact apoA-I is probably in an α-helical conformation that is stabilized by other helices of the molecule (*18*).

In contrast to other peptides of apoA-I studied by our group, which do not self-associate [e.g., [1−44]apoA-I (*21*), [99−143]apoA-I (*26*), and [121−164]apoA-I (*25*)] or have a weak tendency to form dimer [e.g., [143−186]apoA-I (*40*)], [198−243]apoA-I strongly self-associates as the concentration increases and folds into ∼50% α-helical structure. The self-associated [198−243]apoA-I is mainly tetramer and pentamer, as determined by cross-linking. However, native electrophoresis yielded only one band corresponding to a tetramer, and general unfolding data suggested the existence of multiple oligomers with equilibrium toward tetramer as the most stable species. Thus, the C-terminal region of residues 198−243 probably self-associates into tetramer and thus is likely responsible for the self-association of apoA-I, which also self-associates into tetramer (*41*). This is also consistent with investigations using peptides of apoA-I (*23*, *24*) and reports from a number of apoA-I terminal truncation studies by other groups. In solution, [44−186]apoA-I was reported to exist predominantly as a dimer (*10*); [1−192]-apoA-I existed only as monomers and dimers (*7*), and the carboxyl-terminal deletion mutants [1−184]apoA-I and [1−208]apoA-I did not form higher-order aggregates (*8*). Interestingly, the self-association of the peptide starts at ∼2 μM (0.01 mg/mL) and reaches its maximal helical structure

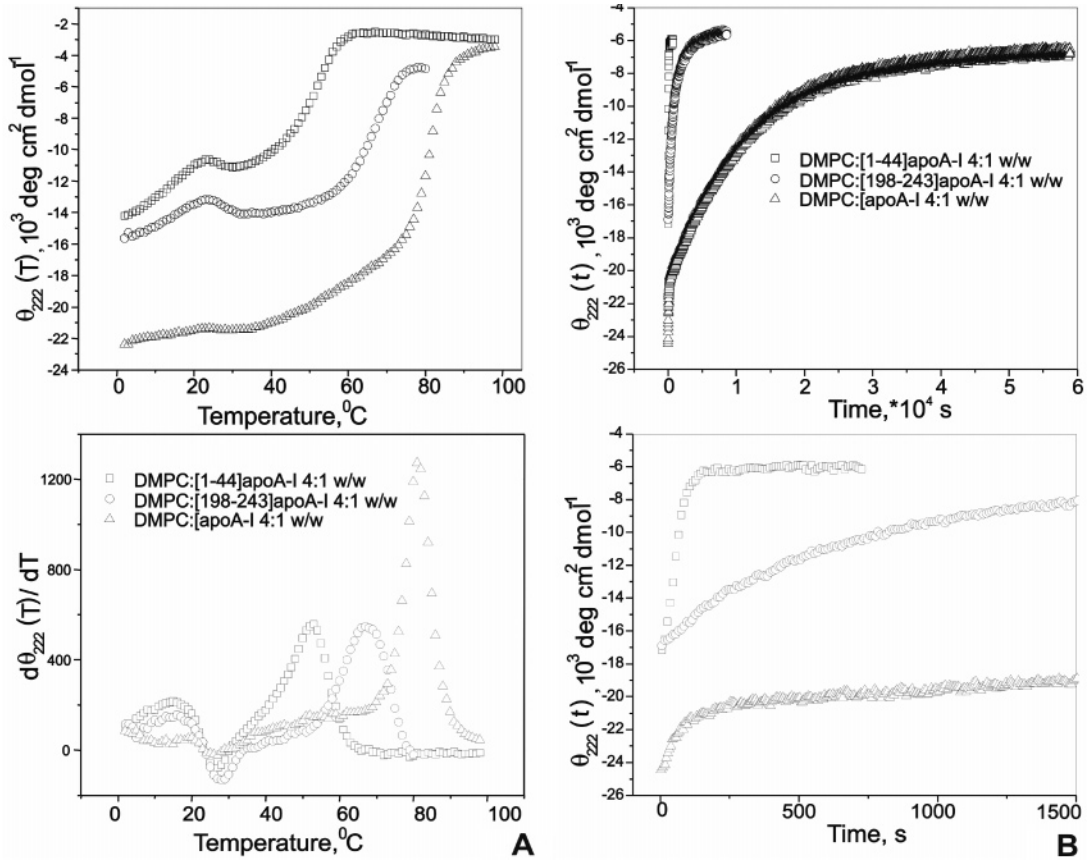

FIGURE 8: (A) Comparison of thermal unfolding [$\theta_{222}(T)$] of complexes formed by [1−44]apoA-I, [198−243]apoA-I, and plasma A-I with DMPC. The samples were 4:1 (w/w) lipid−peptide or lipid−protein complexes for all, prepared at monomeric peptide or protein concentrations. The scanning rate was 0.0033 K/s (300 s/K) for all. The top panel shows thermal unfolding heating curves of the three samples; the bottom panel shows their corresponding differential analysis that yielded the apparent T_m. (B) Comparison of temperature-jump data [$\theta_{222}(t)$] of complexes formed by [1−44]apoA-I, [198−243]apoA-I, and plasma A-I with DMPC. Samples were prepared at monomeric peptide or protein concentrations. The $\theta_{222}(t)$ spectra were recorded every 10 s. The top panel shows temperature-jump data of the three samples in full length; the first 2000 s of those spectra is amplified in the bottom panel.

at ∼20 μM (0.1 mg/mL), as suggested by the formation of maximum α-helical structure at this concentration (Figure 1). In contrast, apoA-I starts to self-associate at ∼40 μM (0.1 mg/mL) (*41*), a molar concentration 20-fold higher than that of [198−243]apoA-I. Thus, the self-association of [198−243]apoA-I is stronger than that of intact apoA-I. This suggests that the self-association of apoA-I through C-terminal interactions is probably modified by interaction of the C-terminus with other regions of the sequence.

The demonstration that this region of the sequence forms an independent helical hairpin domain in the recently determined crystal structure of apoA-I supports our suggestions that the extreme C-terminal 46 residues of apoA-I may function independently and can mimic the self-association and lipid interaction of the intact apoA-I.

As demonstrated by far-UV CD spectra and thermal unfolding data at different peptide concentrations, the self-association of [198−243]apoA-I is an equilibrium between monomer and the multiple self-associated states. The equilibrium moves toward tetramer as the peptide concentration increases. Interestingly, maximum helical structure was observed at and above 0.1 mg/mL (Figure 1), whereas the tetrameric form of the peptide was predominant only at and above 1 mg/mL (Figure 3). This suggests that higher-order oligomer association (e.g., tetramer) does not induce additional secondary structural folding in the peptide compared to lower-order species (e.g., dimer). However, the stability of higher-order oligomer species increased dramatically, as demonstrated by the increase in their T_m values (Figure 3). The T_m of [198−243]apoA-I at ∼1 mg/mL, when the peptide is mainly in tetramer, is ∼97 °C (Figure 3C). This is ∼35 °C higher than that of lipid-free apoA-I in the monomeric form (*42*). Thus, the intermolecular interactions between the tetrameric [198−243]apoA-I are much stronger than the intramolecular interactions between different putative helix repeats in apoA-I that folds ∼60% of the protein into α-helical structure.

Interaction with Lipid-Mimicking Detergents. Like other apolipoproteins and their peptide models, [198−243]apoA-I folded into α-helical structure in the presence of a number lipid-mimicking detergents (BOG, DPC, DHPC, and SDS) and protein folding reagents (TFE) (data not shown).

In contrast to all the other detergents (BOG, DPC, and DHPC) that were investigated that induce α-helix formation in the peptides at and above the detergent CMC, SDS induces α-helical structure formation in [198−243]apoA-I at micromolar concentrations (∼35 μM or 0.001%), 100-fold lower than its typical CMC [∼0.17−0.23% or 6−8 mM (*36*)]. This is also the observation for other apolipoproteins and their peptide models (0.002% for [1−44]apoA-I and 0.04% for [143−186]apoA-I, data not shown). SDS has been reported to induce α-helical structure in membrane proteins at concentrations above its typical CMC (*43*). It is usually thought that α-helical structure in apolipoproteins induced

by SDS is also concomitant with the formation of SDS micelles (*19*). However, our data (Figure 4B) suggest that this ionic detergent induces the formation of α-helical structure in apolipoproteins probably through specific binding, which is different from that of nonionic or zwitterionic detergent (i.e., BOG, DPC, and DHPC). In addition, SDS was reported to induce formation of α-helical structure in the peptide of a membrane protein at a 1:1000 SDS:peptide molar ratio (*44*) and was proposed to be a "catalytic inducer" of α-helices. The mechanism of how SDS folds apolipoproteins into helix requires further investigation.

Lipid Interaction. Both monomeric and self-associated peptide that contains ∼50% α-helix can clear turbid DMPC suspensions over a wide range of lipid:peptide ratios from 1:1 to 10:1 (w/w). At ≥4:1 ratios, no free peptide was observed, and both peptide and lipid were enriched in the density range of 1.08−1.12 g/cm^3, typical of apoA-I−DMPC discoidal complexes. This is in contrast to the N-terminal peptide ([1−44]apoA-I), in which free [1−44]apoA-I always coexists with complexes even in excess DMPC (*21*). Thus, consistent with its proposed high lipid affinity, the C-terminal segment ([198−243]apoA-I) possesses a higher lipid affinity than the N-terminal segment of apoA-I. The high lipid affinity of [198−243]apoA-I is also supported by the observation that complexes formed by the C-terminal peptide with DMPC are significantly more stable than the N-terminal peptide, as demonstrated by both the higher apparent T_m (Figure 8A) and longer unfolding rate (Figure 8B).

At the self-associated concentration, [198−243]apoA-I formed two types of complexes with DMPC depending on the initial DMPC:peptide ratio, small discoidal complexes with a density of ∼1.1 g/cm^3, a weight ratio of ∼3:1 (∼23:1 molar ratio), and a size of ∼110 Å (Figure 6A) and large discoidal complexes with a density of ∼1.085 g/cm^3, a weight ratio of ∼4.6:1 (∼36:1 molar ratio), and a size of ∼165 Å (Figure 6B). The calculated compositions were 8 peptide molecules and 200 DMPC molecules for the small disks and 14 peptide molecules and 500 DMPC molecules for the large ones. The total number of peptide molecules per particle for both types of complexes was consistent with the cross-linking study (Figure 7).

Considering the α-helical content of the peptide in the lipid-bound form is ∼60%, the total helix length per disk can be calculated to be ∼340−425 Å for the small disk (∼110 Å, 8−10 peptide molecules per particle, Figure 6A) and ∼595−765 Å for the large disk (∼165 Å, 14−18 peptide molecules per particle, Figure 6B). These helix lengths can be compared to the perimeter of the lipid component of the disk, namely, ∼280 and ∼450 Å, respectively. Thus, total helix length is more than sufficient to cover the disk edge with a single belt but somewhat shorter than that required for a continuous helical double belt. However, binding of unstructured regions of the peptide(s) to the disk edge may compensate for the lack of helical conformation. In contrast to the ∼100 Å disklike complex formed by the N-terminal peptide ([1−44]apoA-I) in which helical structure was insufficient to cover the disk edge even by a single belt (*21*), the compositions of complexes formed by the C-terminal peptide are more consistent with a "double-belt" model, similar to that proposed for full-length apoA-I (*45*, *46*).

The characteristics (density, weight ratio, size, composition, and total helix length per particle) of the two types of disks formed by the peptide are similar to those of the disks formed by the intact apoA-I under similar conditions (*32*, *39*). This suggests that the C-terminal peptide can mimic the phospholipid interaction of intact apoA-I, also supporting the high lipid affinity of this peptide. Thus, this segment of apoA-I may play a critical role in initiating phospholipid binding in the formation of nascent discoidal HDL. However, the stability of complexes formed by the peptide is much lower than that of apoA-I, as demonstrated by the apparent T_m (Figure 8A) and unfolding rate (Figure 8B). This suggests that the interaction among the putative interhelix repeats is important for intact apoA-I cooperatively binding with phospholipids and stabilizing the complexes.

Interestingly, at monomeric concentrations, when the C-terminal peptide ([198−243]apoA-I) is fully unstructured, a different disk-like complex was formed. Specifically, at an initial lipid:peptide ratio of 1:1 (w/w), the peak fraction density was ∼1.085 g/cm^3, with a weight ratio of ∼4:1 and a size distribution of ∼103 ± 20 Å (data not shown). These values were identical to those of the complex formed by DMPC with the fully unstructured N-terminal peptide ([1−44]apoA-I) under similar conditions (*21*). The calculated composition of this disklike complex contains only enough helix to wrap the phospholipid bilayer once. This suggests that monomeric unstructured N- and C-terminal peptides may interact with phospholipid in a different manner, as compared to the prehelical structured self-associated conformation of the C-terminal peptide ([198−243]apoA-I). The disklike structure may be a "micelle-like" complex with the peptide randomly distributed and creating curvature at the surface of the phospholipid "bilayer". The interaction and the organization between the monomeric peptide and DMPC may be similar to that of apolipoproteins with the phospholipid monolayer at the surface of mature spherical HDL, whereas the interaction of the prefolded and paired α-helical conformation of the self-associated C-terminal peptide with DMPC possibly represents the interaction of apolipoproteins with the phospholipid bilayer disk in the nascent discoidal HDL.

REFERENCES

1. Brouillette, C. G., et al. (2001) Structural models of human apolipoprotein A-I: A critical analysis and review, *Biochim. Biophys. Acta 1531* (1−2), 4−46.
2. Gursky, O. (2005) Apolipoprotein structure and dynamics, *Curr. Opin. Lipidol. 16* (3), 287−294.
3. Sorci-Thomas, M. G., and Thomas, M. J. (2002) The effects of altered apolipoprotein A-I structure on plasma HDL concentration, *Trends Cardiovasc. Med. 12* (3), 121−128.
4. Sorci-Thomas, M. G., et al. (2000) Single repeat deletion in ApoA-I blocks cholesterol esterification and results in rapid catabolism of Δ6 and wild-type ApoA-I in transgenic mice, *J. Biol. Chem. 275* (16), 12156−12163.
5. Rogers, D. P., et al. (1998) Structural analysis of apolipoprotein A-I: Effects of amino- and carboxy-terminal deletions on the lipid-free structure, *Biochemistry 37* (3), 945−955.
6. Gorshkova, I. N., et al. (2002) Lipid-free structure and stability of apolipoprotein A-I: Probing the central region by mutation, *Biochemistry 41* (33), 10529−10539.
7. Ji, Y., and Jonas, A. (1995) Properties of an N-terminal proteolytic fragment of apolipoprotein AI in solution and in reconstituted high density lipoproteins, *J. Biol. Chem. 270* (19), 11290−11297.
8. Laccotripe, M., et al. (1997) The carboxyl-terminal hydrophobic residues of apolipoprotein A-I affect its rate of phospholipid binding and its association with high density lipoprotein, *J. Biol. Chem. 272* (28), 17511−17522.

9. Huang, W., et al. (2000) A single amino acid deletion in the carboxy terminal of apolipoprotein A-I impairs lipid binding and cellular interaction, *Arterioscler. Thromb. Vasc. Biol. 20* (1), 210−216.
10. Beckstead, J. A., et al. (2005) Combined N- and C-terminal truncation of human apolipoprotein A-I yields a folded, functional central domain, *Biochemistry 44* (11), 4591−4599.
11. McLachlan, A. D. (1997) Repeated helical pattern in apolipoprotein-A-I, *Nature 267* (5610), 465−466.
12. Boguski, M. S., et al. (1986) Evolution of the apolipoproteins. Structure of the rat apo-A-IV gene and its relationship to the human genes for apo-A-I, C-III, and E, *J. Biol. Chem. 261* (14), 6398−6407.
13. Luo, C. C., et al. (1986) Structure and evolution of the apolipoprotein multigene family, *J. Mol. Biol. 187* (3), 325−340.
14. Boguski, M. S., et al. (1986) On computer-assisted analysis of biological sequences: Proline punctuation, consensus sequences, and apolipoprotein repeats, *J. Lipid Res. 27* (10), 1011−1034.
15. Nolte, R. T., and Atkinson, D. (1992) Conformational analysis of apolipoprotein A-I and E-3 based on primary sequence and circular dichroism, *Biophys. J. 63* (5), 1221−1239.
16. Segrest, J. P., et al. (1992) The amphipathic helix in the exchangeable apolipoproteins: A review of secondary structure and function, *J. Lipid Res. 33* (2), 141−166.
17. Rogers, D. P., et al. (1997) Truncation of the amino terminus of human apolipoprotein A-I substantially alters only the lipid-free conformation, *Biochemistry 36* (2), 288−300.
18. Gorshkova, I. N., et al. (2000) Probing the lipid-free structure and stability of apolipoprotein A-I by mutation, *Biochemistry 39* (51), 15910−15919.
19. Okon, M., et al. (2002) Heteronuclear NMR studies of human serum apolipoprotein A-I. Part I. Secondary structure in lipid-mimetic solution, *FEBS Lett. 517* (1−3), 139−143.
20. Oda, M. N., et al. (2003) The C-terminal domain of apolipoprotein A-I contains a lipid-sensitive conformational trigger, *Nat. Struct. Biol. 10* (6), 455−460.
21. Zhu, H. L., and Atkinson, D. (2004) Conformation and lipid binding of the N-terminal (1−44) domain of human apolipoprotein A-I, *Biochemistry 43* (41), 13156−13164.
22. Ajees, A. A., et al. (2006) Crystal structure of human apolipoprotein A-I: Insights into its protective effect against cardiovascular diseases, *Proc. Natl. Acad. Sci. U.S.A. 103* (7), 2126−2131.
23. Palgunachari, M. N., et al. (1996) Only the two end helixes of eight tandem amphipathic helical domains of human apo A-I have significant lipid affinity. Implications for HDL assembly, *Arterioscler. Thromb. Vasc. Biol. 16* (2), 328−338.
24. Mishra, V. K., et al. (1998) Studies of synthetic peptides of human apolipoprotein A-I containing tandem amphipathic α-helixes, *Biochemistry 37* (28), 10313−10324.
25. Wally, J. (2004) Conformation and lipid binding properties of peptide models of exchangeable apolipoproteins, Ph.D. Thesis, Boston University, Boston.
26. Chao, Y. (2003) Conformational studies of a consensus sequence peptide (CSP) and a real sequence peptide (RSP) of apolipoproteins by circular dichroism spectroscopy and X-ray crystallography, Ph.D. Thesis, Boston University, Boston.
27. Dong, L., and Atkinson, D. (2005) Structure and stablity of a consensus sequence (CSP-BABA) of apolipoproteins, *Protein Sci. 14* (Suppl. 1).
28. Gursky, O. (2001) Solution conformation of human apolipoprotein C-1 inferred from proline mutagenesis: Far- and near-UV CD study, *Biochemistry 40* (40), 12178−12185.
29. Fang, Y., Gursky, O., and Atkinson, D. (2003) Structural studies of N- and C-terminally truncated human apolipoprotein A-I, *Biochemistry 42* (22), 6881−6890.
30. Mao, D., and Wallace, B. A. (1984) Differential light scattering and absorption flattening optical effects are minimal in the circular dichroism spectra of small unilamellar vesicles, *Biochemistry 23* (12), 2667−2673.
31. Swaney, J. B., and O'Brien, K. (1978) Cross-linking studies of the self-association properties of apo-A-I and apo-A-II from human high density lipoprotein, *J. Biol. Chem. 253* (19), 7069−7077.
32. Fang, Y., Gursky, O., and Atkinson, D. (2003) Lipid-binding studies of human apolipoprotein A-I and its terminally truncated mutants. *Biochemistry 42* (45), 13260−13268.
33. Janiak, M. J., Small, D. M., and Shipley, G. G. (1979) Temperature and compositional dependence of the structure of hydrated dimyristoyl lecithin, *J. Biol. Chem. 254* (13), 6068−6078.
34. Schellman, J. A. (1997) Temperature, stability, and the hydrophobic interaction, *Biophys. J. 73* (6), 2960−2964.
35. Lorber, B., Bishop, J. B., and DeLucas, L. J. (1990) Purification of octyl β-D-glucopyranoside and re-estimation of its micellar size, *Biochim. Biophys. Acta 1023* (2), 254−265.
36. Reynolds, J. A., et al. (1967) The binding of diverse detergent anions to bovine serum albumin, *Biochemistry 6* (3), 937−947.
37. Otzen, D. E. (2002) Protein unfolding in detergents: Effect of micelle structure, ionic strength, pH, and temperature, *Biophys. J. 83* (4), 2219−2230.
38. Otzen, D. E., and Oliveberg, M. (2002) Burst-phase expansion of native protein prior to global unfolding in SDS, *J. Mol. Biol. 315* (5), 1231−1240.
39. Jonas, A., Kezdy, K. E., and Wald, J. H. (1989) Defined apolipoprotein A-I conformations in reconstituted high density lipoprotein discs, *J. Biol. Chem. 264* (9), 4818−4824.
40. Zhu, H. L. (2006) Structure, interaction and lipid binding of subdomains of human apolipoprotein A-I, Ph.D. Thesis, Boston University, Boston.
41. Teng, T. L., et al. (1977) An ultracentrifugal study of the self-association of canine apolipoprotein A-I in solution, *J. Biol. Chem. 252* (23), 8634−8638.
42. Mehta, R., Gantz, D. L., and Gursky, O. (2003) Human plasma high-density lipoproteins are stabilized by kinetic factors, *J. Mol. Biol. 328* (1), 183−192.
43. Montserret, R., et al. (2000) Involvement of electrostatic interactions in the mechanism of peptide folding induced by sodium dodecyl sulfate binding, *Biochemistry 39* (29), 8362−8373.
44. Micelli, S., et al. (2004) Effect of nanomolar concentrations of sodium dodecyl sulfate, a catalytic inductor of α-helices, on human calcitonin incorporation and channel formation in planar lipid membranes, *Biophys. J. 87* (2), 1065−1075.
45. Segrest, J. P., et al. (1999) A detailed molecular belt model for apolipoprotein A-I in discoidal high density lipoprotein, *J. Biol. Chem. 274* (45), 31755−31758.
46. Catte, A., et al. (2006) Novel changes in discoidal high density lipoprotein morphology: A molecular dynamics study, *Biophys. J. 90* (12), 4345−4360.

BI061721Z